



The Motion of a Losing Mass Plasmon

P. R. Rivera-Ortiz^{1,2}, A. Rodríguez-González^{1,2} , L. Hernández-Martínez¹, and J. Cantó³

¹ Instituto de Ciencias Nucleares, Universidad Nacional Autónoma de México, Ap. 70-543, 04510 D.F., México; pedro.rivera@correo.nucleares.unam.mx

² LUTH, Observatoire de Paris, PSL, CNRS, UPMC, Univ Paris Diderot, 5 place Jules Janssen, F-92195 Meudon, France

³ Instituto de Astronomía, Universidad Nacional Autónoma de México, Ap. 70-264, 04510 D.F., México

Received 2018 November 13; revised 2019 January 30; accepted 2019 February 7; published 2019 March 19

Abstract

The interaction of a high velocity clump of gas has been described by the plasmon model, which considers balance between ram pressure and the internal stratified structure of the decelerated clump. In this paper we propose an analytical model to describe the mass loss of such a clump due the interaction with the environment, describing its influence on the plasmon dynamics. We carry out comparisons between an analytic model and axisymmetric gas dynamic simulations of plasmon evolution. From our simulations we were able to find the values of the friction constants α and λ . Comparing with the complete analytic model from which we can infer the position and the mass loss of the clump as a function of the clump's density and the environment ratio.

Key words: ISM: general – ISM: jets and outflows – ISM: kinematics and dynamics – shock waves

1. Introduction

The problem of a wind/molecular cloud interaction has been studied at length in the past. De Young & Axford (1967, hereafter DA) described the motion of a clump decelerated by the ram pressure and determined the lifetime of the plasmon. They applied this model to Cygnus A and concluded that analyzing the dynamics of plasmons should reduce their free parameters. It became a very popular model to explain confinement of radio lobes propagating through the intergalactic medium (Ubachukwu et al. 1991; Daly 1994), models of radio-loud quasars (Daly 1995), and models of the optical narrow-line regions of Seyfert galaxies (Taylor et al. 1992; Veilleux et al. 1993). Cantó et al. (1998; hereafter C98) rederived the plasmon solution, adding the centrifugal pressure to obtain a modified plasmon profile.

In most cases it is difficult to calculate the real age of an astronomical plasmon because there is no clear information about deceleration and most plasmons are isolated so there is not enough information about the static medium. To solve this problem a set of several plasmons with an noticeable deceleration moving under similar restrictions is needed.

Orion BN/KL is an ideal laboratory to prove the plasmon solution, because it has an almost isotropic and explosive outflow that could be produced by the nonhierarchical close dynamic interaction of a forming multiple-star system (Zapata et al. 2009). In this region there are more than a hundred filamentary structures known as fingers that allow us to estimate a dynamical age between 1000 and 500 yr, assuming no deceleration. Nevertheless, there is observational evidence that the longest fingers detected in H₂ emission are losing speed, probing their interaction with the environment (Bally et al. 2011). It is a very interesting star formation region that due to its distance, at 414 pc, allows us to determine its characteristics with enough detail. Therefore, we also can model the physics using theoretical and numerical models, using some observational constrains. Some of these models have achieved important results as determining the dynamical age and the energy of the explosive event. Nevertheless, there are important questions that deserve attention and are not resolved yet, such as the real age of the event, the mechanism

that can generate such distribution of the fingers, as well as their ejection velocity since there is evidence of a drag force.

The effect of a drag force is necessary to understand the real motion of a plasmon. Several numerical simulations have shown a deceleration effect greater than that expected by ram pressure (Yalinewich & Sari 2016), but it has not been deeply analyzed since cooling effects were not included.

The destruction of the original clump was also considered in Raga et al. (1998) in their study of the interaction of a fast wind impinging into a compact spherical cloud. They concluded that the motion is affected by the detachment of material of the cloud, which results in a limited application of their model.

Then, the assumption that a clump has no deceleration or a deceleration according to models with constant mass, can lead to an overestimate of the age of astrophysical outflows.

In this work, we use the DA solution to propose a mass-loss rate for a plasmon and we obtained its equation of motion. We compare results of this analytic model with numerical simulations using Orion BN/KL plausible ejection conditions. We presented analytic (Section 2) and numerical (Section 3) models of a deceleration of the clumps as a function of ratio density when the mass-loss rate is considered. We present a comparison between the analytic and numerical models and a prediction of the lifetime of clumps assuming similar conditions to the system Orion BN/KL in Section 4. Finally, we present our conclusions in Section 5.

2. Analytical Model

2.1. DA's Plasmon

DA studied the problem of a clump of gas moving through a uniform environment. They found a solution (the “plasmon” solution) based on the balance between the ram pressure of the environment and the stratified thermal pressure of the decelerating clump. For a clump of mass M , isothermal sound speed c , moving supersonically with velocity v through a medium of density ρ_a , the plasmon adopts a pressure and density stratification given by

$$P = P_0 e^{-x/h}, \quad \rho = \rho_0 e^{-x/h}, \quad (1)$$

as a function of the position x from the tip of the cloud where the pressure is P_0 , the density is $\rho_0 = P_0/c^2$, where c is the isothermal speed of sound. Ram pressure with the environment with density ρ_a indicates $P_0 = \rho_a v^2$.

In Equation (1)

$$h = \frac{c^2}{a}, \quad (2)$$

is the scaleheight of the pressure distribution, and a is the deceleration of the clump.

The balance between the internal pressure and the ram pressure with the surrounding environment shapes the plasmon as,

$$y = 2h \arctan(e^{x/h} - 1)^{1/2}. \quad (3)$$

Then, the mass of the moving clump of gas is related to the shape by the material enclosed by y ,

$$M = \int_0^\infty \pi \rho y^2 dx = \xi_{\text{DA}} \frac{\rho_a v^2 h^3}{c^2}, \quad (4)$$

where $\xi_{\text{DA}} = \frac{\pi}{2}(\pi^2 - 4)$.

2.2. Mass-loss Rate

We propose a mass-loss rate per unit area, μ , which depends on the density and the internal sound speed, c ,

$$\mu = \lambda \rho c, \quad (5)$$

where λ is an unknown parameter expected to be less than one. Behind Equation (5), there is the assumption that the clump loses mass at a rate per unit area proportional to the local mass density, ρ , and with a subsonic velocity λc . This hypothesis has been proposed and tested, for instance, by Kahn (1980), Cantó & Raga (1991), and Raga et al. (1995) in their studies of the turbulent mixing layers produced by the interaction of interstellar outflows. An estimation of λ , in our case, is found by comparison with our numerical simulation of the problem.

Therefore, the total mass-loss rate is given by the integration of μ over the total surface of the plasmon,

$$\dot{M} = \int_0^\infty \mu dA = \lambda \xi_{\text{DA}} \left(\frac{8}{\pi + 2} \right) \frac{\rho_a v^2 h^2}{c}, \quad (6)$$

Dividing Equation (4) by (6) and using Equation (2) we obtain the differential equation,

$$\frac{1}{M} \frac{dM}{dv} = \frac{8\lambda}{(\pi + 2)c}. \quad (7)$$

We can use a dimensionless version of Equation (7) with the following definitions,

$$m = M/M_0, \quad u = v/v_0, \quad \alpha = \frac{8\lambda v_0}{(\pi + 2)c}, \quad (8)$$

where M_0 is the initial mass and v_0 is the initial velocity of the plasmon. The solution to Equation (7) is

$$m = M_0 e^{-\alpha(1-u)}, \quad (9)$$

which relates that mass behavior as a function of the plasmon speed with the constant α .

The equation of motion of the plasmon is,

$$\frac{dv}{dt} = -a. \quad (10)$$

Solving Equation (4) for h , Equation (2) for a , and substituting in Equation (10), we find the equation of motion in a nondimensional form

$$\frac{du}{d\tau} = -\left(\frac{u^2}{m}\right)^{1/3}, \quad (11)$$

where

$$\tau = t/t_0, \quad t_0 = \left(\frac{M_0 v_0}{\xi_{\text{DA}} \rho_a c^4}\right)^{1/3}. \quad (12)$$

Equation (11), together with Equation (9), has the formal solution,

$$\tau = \int_u^1 u^{-2/3} e^{-\frac{\alpha}{3}(1-u)} du. \quad (13)$$

The position of the clump after ejection R is found by solving the kinematic equation,

$$\frac{dR}{dt} = v. \quad (14)$$

Defining $r = R/(v_0 t_0)$ and combining it with Equation (14), we find the solution

$$r = \int_u^1 u^{1/3} e^{-\frac{\alpha}{3}(1-u)} du. \quad (15)$$

Then Equations (9), (13), and (15) give the mass m , velocity u , and position r of the clump after a time τ of ejection, using u as the free variable in the interval $[0, 1]$.

The clump halts at a finite time τ_f and finite distance r_f with finite mass m_f . These limits are determined by the condition $u = 0$ in Equations (9), (13), and (15) and are functions of α only. We can find useful approximations in the limits $\alpha \ll 1$:

$$\tau_f \simeq 3 \left(1 - \frac{\alpha}{4}\right), \quad (16)$$

$$r_f \simeq \frac{3}{4} \left(1 - \frac{\alpha}{7}\right), \quad (17)$$

which are consistent with the DA solution. Furthermore, for $\alpha = 0$ in Equation (13) and Equation (17) we recover the DA solution.

Also, there are some interesting results concerning the stopping time τ_f and distance r_f that deserve to be highlighted.

First, we must note that independent of the physical characteristics of the original clump (shape, density structure, or internal sound speed), the initial interaction with the medium through which it moves will modify these characteristics to those of a plasmon. That is, its shape will be transformed to that given by Equation (3), its pressure and density stratification given by Equation (1) and so on. This transformation is actually accomplished by a reverse shock that moves inside the original clump, changing it into a plasmon.

As we have seen above the structure of the plasmon is highly dependent on its internal sound speed (i.e., on its temperature). Let us assume that the temperature of the newly formed plasmon is the one left by the reverse shock that moved through it. For simplicity, let us also assume that this shock is planar and strong. In the [Appendix](#) we show that the corresponding

isothermal sound speed is,

$$c = v_0 \left(\frac{\gamma - 1}{2} \right)^{1/2} \beta, \quad (18)$$

where $\beta = \sqrt{\rho_a / \rho_{cl}}$ is the square root of the ratio of the density of the environment and the density of the original clump. Using Equation (18) in (8) we find

$$\alpha = \frac{8\lambda}{\pi + 2} \sqrt{\frac{2}{\gamma - 1}} \left(\frac{1}{\beta} \right), \quad (19)$$

which is independent of the velocity v_0 and depends only on the ratio β . Next, let us consider the time t_f for the clump to stop. It is given by

$$t_f = t_0 \tau_f(\alpha), \quad (20)$$

where t_0 is defined by Equation (12) as,

$$t_0 = \left(\frac{M_0 v_0}{\xi_{DA} \rho_a c^4} \right)^{1/3}, \quad (21)$$

or

$$t_0 = \left[\frac{M_0}{\xi_{DA} \rho_a} \left(\frac{v_0}{c} \right)^4 \right]^{1/3} \frac{1}{v_0}, \quad (22)$$

and corresponds to the timescale used by DA in their solution to estimate the lifetime of a plasmon (Equation (27)).

As shown in the [Appendix](#) (see also Equation (20)) the ratio v_0/c is the only function of the contrast density β and it is independent of the velocity v_0 . Thus, given the ratio β , the time t_0 , and therefore the time t_f for the clump to stop diminish as the initial velocity of the clump increases. This is an unexpected result: the time for stopping a stripping clump is inverse with its initial velocity. Faster clumps stop earlier independent of their size. Now, let us consider the stopping distance R_f . This is given by,

$$R_f = v_0 t_0 \tau_f(\alpha). \quad (23)$$

From the discussion above, the product $v_0 t_0$ results are independent of v_0 , and thus R_f . Then, clumps with the same ratio stop at the same distance from the injection point, independent of either its initial velocity or size.

3. Axisymmetric Simulations of Plasmon Evolution

3.1. The Numerical Setup

In order to validate the analytical model, we have computed axisymmetric numerical simulations with the full radiative gas dynamic equations. We used the WALKIMYA 2D code (see Esquivel et al. 2010; Castellanos-Ramírez et al. 2018) to perform all numerical simulations. The code solves the hydrodynamic equations and chemical networks on a two-dimensional Cartesian adaptive mesh, using a second-order finite volume method with HLLC fluxes (Toro et al. 1994).

The adaptative mesh consists of four root blocks of 16×16 cells, with 7 levels of refinement, yielding a maximum resolution of 4096×1024 (axial \times radial) cells. The boundary conditions used on the symmetry axis are reflective and the other ones are outflows. The size of the mesh is large enough so that the choice of outer boundaries does not affect the simulation.

Table 1
Initial Conditions of the Numerical Models

Models	Environment n_a (cm^{-3})	Clump v_0 (km s^{-1})
M1V300/M1V500	1.0×10^6	300/500
M2V300/M2V500	3.16×10^6	300/500
M3V300/M3V500	1.0×10^7	300/500
M4V300/M4V500	3.16×10^7	300/500
M5V300/M5V500	1.0×10^8	300/500

The energy equation includes the cooling function described by Raga & Reipurth (2004) for atomic gas and for lower temperatures we have included the parametric molecular cooling function presented in Kosiński & Hanasz (2007),

$$\Lambda_{\text{mol}}(T) = L_1 \cdot T^{\epsilon_1} + L_2 \cdot \exp\left(-\frac{c_*}{(T - T_*)^{\epsilon_2}}\right), \quad (24)$$

for $T < 5280$ K, where, $L_1 = 4.4 \times 10^{-67} \text{ erg cm}^3 \text{ s}^{-1} \text{ K}^{-\epsilon_1}$, $L_2 = 4.89 \times 10^{-25} \text{ erg cm}^3 \text{ s}^{-1}$, $c_* = 3.18 \text{ K}^{-\epsilon_2}$, $\epsilon_1 = 10.73$, $\epsilon_2 = 0.1$, and $T_* = 1$. K. The total radiative energy for temperatures lower than 5280 K is given by,

$$L_{\text{rad,mol}} = n_{\text{gas}} \cdot n_{\text{CO}} * \Lambda_{\text{mol}}(T), \quad (25)$$

where n_{gas} and n_{CO} are the numerical density of the gas and the CO molecule, respectively.

We have also considered the heating of the gas via cosmic rays, using the heating rate presented in Henney et al. (2009),

$$\Gamma_{\text{crp}} = 5 \times 10^{-28} n_{\text{H}}, \quad (26)$$

where n_{H} is the numerical density of the all the hydrogen species.

3.2. Numerical Models of the Plasmon Evolution

In order to study the deceleration of a high velocity clump we use compatible parameters with the ejection of Orion Fingers in Orion BN/KL. We have run a numerical simulation assuming that the computational domain was initially filled by a homogeneous, stationary ambient medium with temperature $T_{\text{env}} = 100$ K and various densities (see below). The numerical integration had a domain with a physical size of $48,000 \times 12,000$ au on each side, with a maximum resolution (along the two axes) of 11.7 au. We carried out time integration from $t_i = 0$ to $t_f = 1000$ yr, and the clump is released at $z = 700$ au for all models. An estimation of the initial mass in each of the clumps is $m_{\text{cl}} = 0.03 M_{\odot}$ since the total mass of the moving gas in the ~ 400 fingers in Orion BN/KL is about $8 M_{\odot}$ (Bally 2016). Also, the observed transverse size of the fingers is about 400 au.

In the numerical models, the initial clump is imposed in a sphere of radius $R_{\text{cl}} = 50$ au, corresponding to 4 pixels at the maximum resolution of the adaptive grid and with a uniform density of $n_{\text{cl}} = 1 \times 10^{10} \text{ cm}^{-3}$. Since the initial clump is out of equilibrium, it increases its size to about 400 au from the first output, and then the density structure of a plasmon arises.

We have computed 10 simulations of the clumps, varying the density of the interstellar medium and the velocity at which the clump was thrown (see Table 1).

One of the main hypotheses of our analytic model is that the early interaction of the original clump with the environment will modify its initial characteristics (shape, density

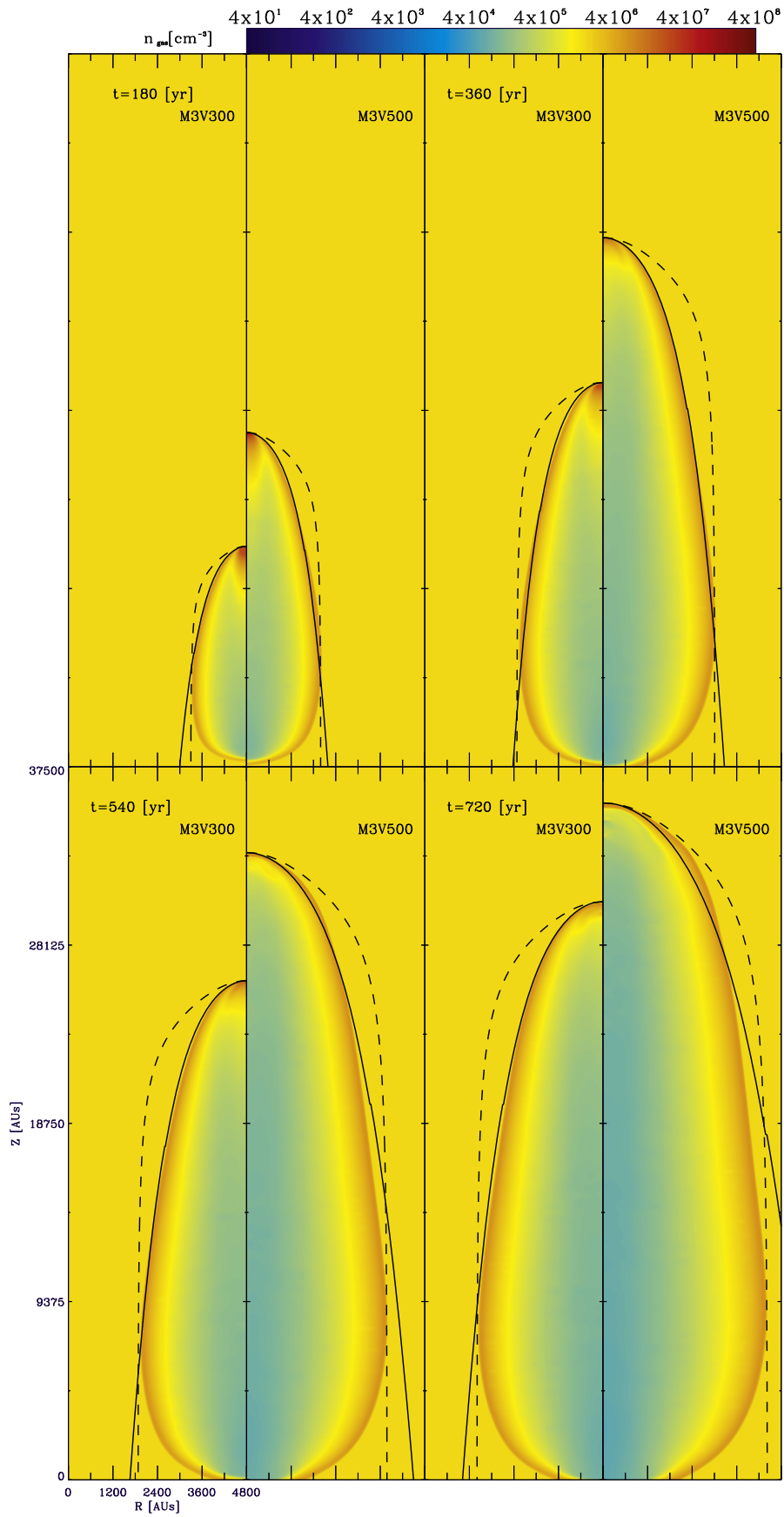


Figure 1. Snapshots from the numerical simulations showing the numerical density. Each panel compares two models with initial velocities of 300 (left) and 500 (right) km s^{-1} at $t = 180, 360, 540,$ and 720 yr. Lines are the analytical fit; dashed lines are those of DA and solid lines are ours.

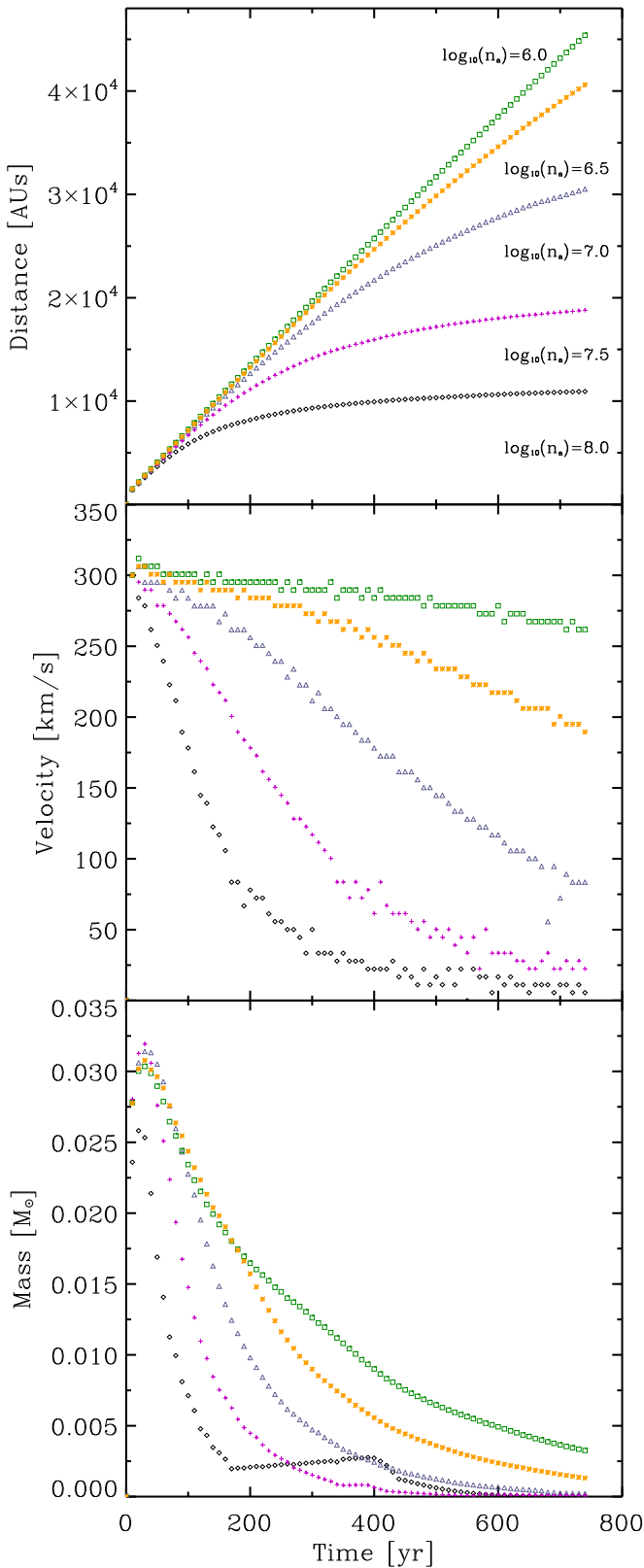


Figure 2. Top, middle, and bottom panels show the position, velocity, and mass as functions of time by the numerical model with initial velocities of 300 km s^{-1} , respectively. In each of the panels we plot the results obtained for the models evolving with logarithmic interstellar medium densities of 6, 6.5, 7, 7.5, and 8 using green squares, yellow asterisks, blue triangles, magenta crosses, and black diamond symbols, respectively.

stratification, or sound speed) to those of a plasmon. The sound speed of the moving clump is calculated using the internal temperature, which is about 15 K and is on the order of magnitude of the sound speed obtained with Equation (42).

In order to illustrate the numerical simulation results, in Figure 1 we present the density maps for models M3V300 and M3V500 (left and right panels, respectively) at evolutionary time of 180, 360, 540, and 720 yr, top left, top right, bottom left, and bottom right panels, respectively. The solid lines, in all the panels, are the analytical fit of the plasmon shape, Equations (16) and (17) presented in C98 and the dashed lines are also the plasmon shape's fit obtained by DA in their Equation (2). In both models, the plasmon shape expected by the DA equation is wider than the shape of the plasmon's head obtained in the numerical simulations. For model M3V500 (the right panels of Figure 1) the plasmon shape proposed by C98 is in very good agreement with the numerical simulations, at least up to $t \sim 500 \text{ yr}$. After this time, the plasmon (of the model M5V300) is rapidly decelerated and the bow shock changes in a different shape than that proposed by C98. The model with lower initial velocity, model M3V300, does not have an appreciable deceleration and the numerical simulation shape is in agreement with the C98 prediction.

Another prediction of our model is that the dimensionless mass m of the clump is related to its dimensionless velocity u by Equation (9). We can test this prediction. The top panel of Figure 2 shows the position as a function of time by plasmon for the models with initial velocities of 300 km s^{-1} (see Table 1). The squares, asterisks, triangles, and plus and diamond symbols represent the results obtained for the models evolving with logarithmic interstellar medium densities of 6, 6.5, 7, 7.5, and 8, respectively. As we can see, the position is smaller for models evolving in denser environments, which means the deceleration or decrease of the plasmon's velocity, as a function of time (see the middle panel of Figure 2), is larger in models with larger ram pressure (Equation (34)). In the bottom panel of this figure, we presented the mass of the clump as a function of time. We calculated the mass, considering the gas inside the sphere of 50 au of radii from the clump position, and we also note that the denser interstellar medium produces a larger mass-loss rate in the clumps moving in environments with uniform density and temperatures. In the same way, Figure 3 shows the position, velocity, and mass as functions of time of the numerical simulations, which we considered for a larger initial velocity, 500 km s^{-1} . The results of the distance, velocity, and mass are very similar to those found in the models with initial velocity of 300 km s^{-1} . However, the deceleration for the models with initial velocities of 500 km s^{-1} is larger than those for the models with $v_0 = 300 \text{ km s}^{-1}$, and the lifetime of the faster clumps is smaller than those for the lower ones, as we predicted in our Equation (22).

Using the dimensionless mass of the clump and velocity from our numerical simulation in Equation (13) we fitted the α value for all the numerical models. Figure 4 shows the logarithm of the mass of the clump as a function of velocity (dimensionless), for all the models with initial velocities of 300 km s^{-1} , we use the same nomenclature for the symbols as in the Figure 2, and the solid lines are the fits for the models, M1V300, M2V300, M3V300, M4V300, M5V300, and M6V300.

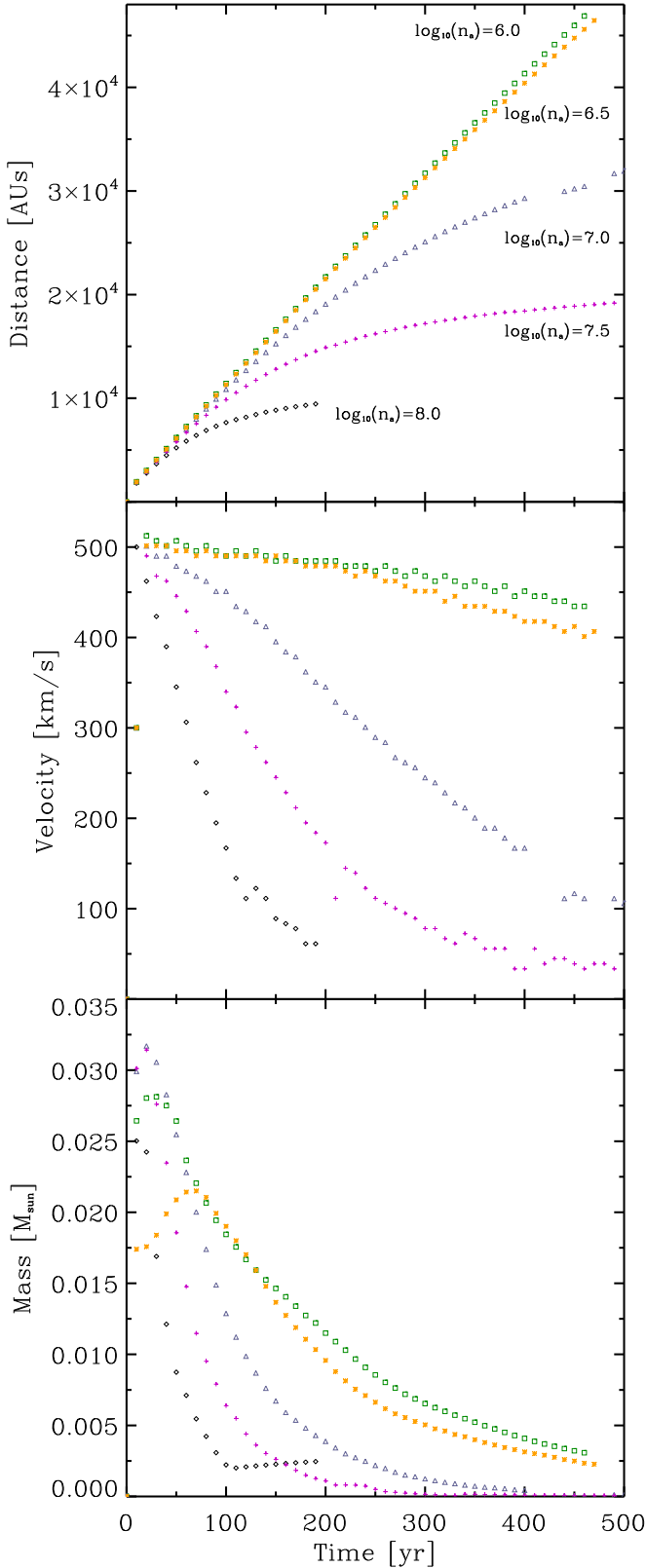


Figure 3. Same as Figure 2 but for models with initial velocity of 500 km s^{-1} .

The α values for all the models presented here are plotted in Figure 5. The plus and diamond symbols are the α values fitted for modes with $v_0 = 300$ and 500 km s^{-1} , respectively. In order to obtain the value for the constant λ (see Equation (19)), we have fitted the α values as functions of the contrast density

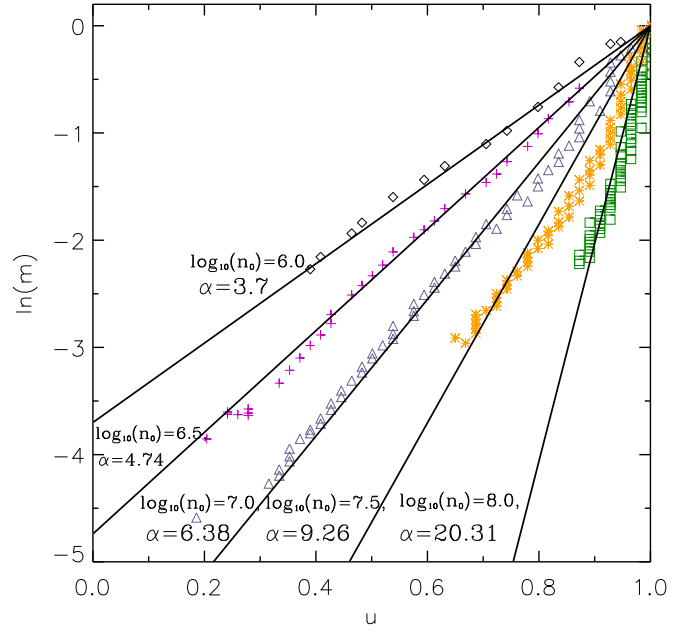


Figure 4. Mass of the clump as a function of the clump's velocity (dimensionless). The nomenclature of the symbols is the same as in Figure 2 and in solid lines we plot the fit for each of the models with initial velocities of 300 km s^{-1} .

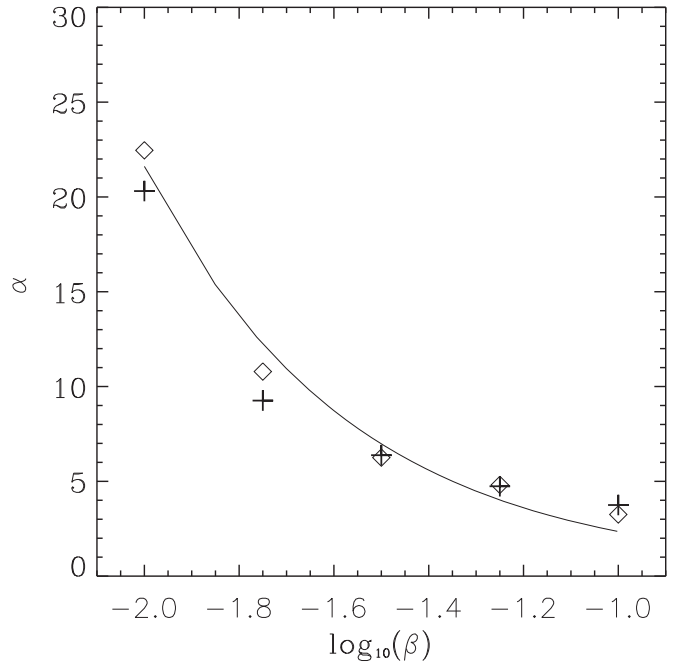


Figure 5. Constant α as a function of contrast density (β). The plus and diamond symbols are the α values for models with $v_0 = 300$ and 500 km s^{-1} , respectively, and the solid line is the best fit of λ (see Equation (19)), $\lambda = 0.0615$.

β to our numerical simulation (solid line in this figure). The best fit gives $\lambda = 0.0615$. Notice that the α values are only functions of contrast density and these values are not dependent on the initial velocity or other parameters of the cloud, as described by Equation (19). λ is a constant that is independent of the physical properties of the interstellar medium or clump gas.

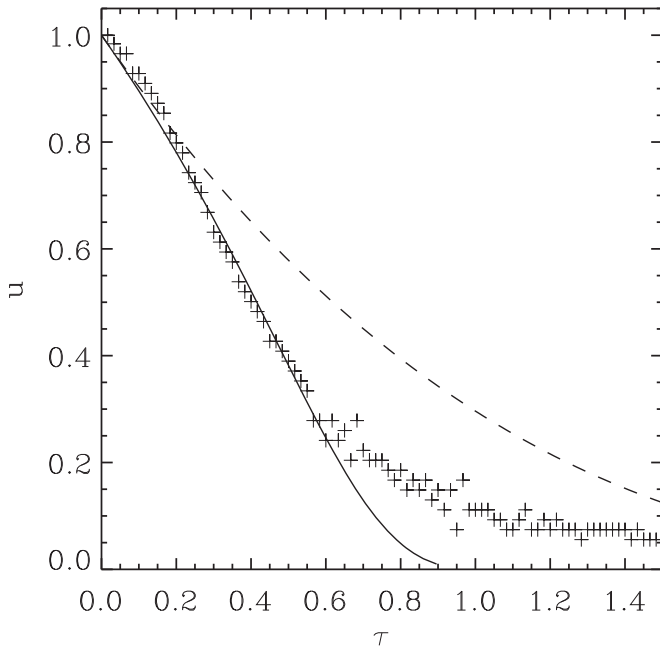


Figure 6. Dimensionless velocity, u , vs. dimensionless time, τ , for the model with $\log \beta = -1.25$. Solid line represents the solution to Equation (13), dashed line is the De Young and Axford prediction in Equation (27) and crosses are the numerical simulation data normalized with $v_0 = 300 \text{ km s}^{-1}$ and $t_0 = 600 \text{ yr}$.

4. Prediction of Evolutionary Physical Properties of the Plasmon

The solution for a constant mass plasmon can be found from, Equation (13) with $\alpha = 0$. The results are a dimensionless velocity

$$u = \left(1 - \frac{\tau}{3}\right)^3, \quad (27)$$

and, dimensionless position

$$r = \frac{3}{4} \left[1 - \left(1 - \frac{\tau}{3}\right)^4\right]. \quad (28)$$

Therefore, in the approximation of DA, the lifetime of a plasmon is $t_f = 3 \cdot t_0$ (see Equation (27)). When a mass-loss rate is taken into account the plasmon's motion is changed, and Equation (13) can be integrated numerically to obtain u and the dimensionless position $r = x/x_0$ with $x_0 = v_0 t_0$. It is important to recall that C98 included the centrifugal pressure, which can affect the plasmon shape. This effect was not included in DA or our work.

Finally, we use our numerical simulations to probe our models and their limitations. Each simulation has physical units, so they have to be normalized with v_0 , t_0 , and x_0 . v_0 is obtained directly from the initial conditions, t_0 is obtained from a fit of the velocity data, and x_0 comes from a similar fit of the position data.

Figure 6 shows the dimensionless velocity as a function of dimensionless time. From this figure, one can see that the DA solution, represented with a dashed line, agrees $\tau \leq 0.2$ to the values obtained from the numerical model M4V300, marked as cross symbols. However, the semianalytical solution, the solid line, is in agreement with the numerical model up to $\tau = 0.6$. Note that after $\tau = 0.6$ the values of u , for the numerical simulation, tend to be constant. There are numerical

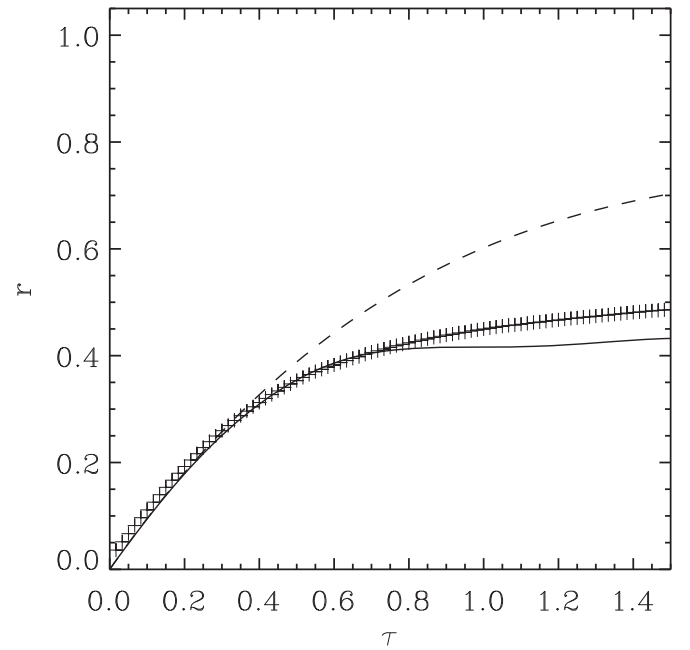


Figure 7. Dimensionless position, r , vs. dimensionless time, τ , for the model with $\log \beta = -1.25$. The solid line represents the solution to Equation (13), the dashed line is the De Young and Axford prediction in Equation (28) and crosses are the numerical simulation data normalized with $x_0 = 38,000 \text{ au}$ and $t_0 = 600 \text{ yr}$.

uncertainties that lead us to overestimate the velocity, since, as the plasmon loses mass, it is difficult to determine its position and therefore its velocity.

Figure 7 shows the dimensionless position as a function of dimensionless time. The DA solution, semianalytic solution, and numerical data are represented as in Figure 6. The DA solution is similar to numerical data for $\tau \leq 0.4$ while for the semianalytical solution this time is as long as $\tau = 0.8$. Nevertheless, semianalytic has a similar stop distance while the DA model predicts a larger distance.

Finally, the analytic t_0 and $x_0 = v_0 t_0$ obtained from Equation (12) and the numerical t_0 and x_0 , for all the models presented in this job, are also tabulated. Tables 2 and 3 presented the final position (scale length) and lifetimes (scale time) of our models with initial velocities of 300 and 500 km s^{-1} , respectively.

From the analytical solution, we can see that the final position (the scale length) is the only function of the contrast density and it is not related to the velocity at which the clump was thrown, see Tables 2 and 3. However, the lifetime of the plasmon or clump is related with the initial velocity and the density contrast, the plasmon pushed with more velocity reach the final size before the plasmon with lower initial velocities. That is, the plasmons that were faster initially suffer a higher deceleration.

Nevertheless, the numerical simulation does not predict the position of the plasmon when the velocity is equal to zero; therefore, the x_0 and t_0 values follow the same trend but only in the order of magnitude of the analytic predictions.

5. Conclusions

We have used the plasmon solution obtained by DA and the solution presented in C98 to propose an analytical solution of the plasmon's deceleration when a mass-loss rate is considered.

Table 2
Analytic and Numerical Scale Length x_0 and Time t_0 for Models with $v_0 = 300 \text{ km s}^{-1}$

$\log\left(\frac{n_a}{(\text{cm}^{-3})}\right)$	Analytical		Numerical	
	x_0 (au)	t_0 (yr)	x_0 (au)	t_0 (yr)
6	1.14×10^6	18,369	1.2×10^6	18,400
6.5	363,868	5868	200,000	3000
7.0	117,000	1900	90,000	1400
7.5	38,231	616	38,000	600
8	12,762	205	18,000	250

Table 3
Analytic and Numerical Scale Length x_0 and Time t_0 for Models with $v_0 = 500 \text{ km s}^{-1}$

$\log\left(\frac{n_a}{(\text{cm}^{-3})}\right)$	Analytical		Numerical	
	x_0 (au)	t_0 (yr)	x_0 (au)	t_0 (yr)
6	1.14×10^6	11,022	1.1×10^6	10,000
6.5	363,868	3500	300,000	2700
7.0	117,000	1134	90,000	850
7.5	38,231	370	40,000	400
8	12,762	123	19,000	165

This leads to interpreting mass as a function of the plasmon velocity related by a constant α . This α can be interpreted as a friction coefficient. We calculate its dependence on the density contrast between the plasmon and the surrounding environment.

Several numerical simulations were performed trying to compare the validity of our analytic model, and the constant α and λ were obtained from the results. An estimation of $\lambda = 0.0615$ was found.

The lifetime obtained from the simple plasmon model is greater than that expected by our losing mass considerations. The deceleration obtained by this method is more likely to be responsible for the age discrepancy in astronomical flows as the Orion fingers. Also, it is important to notice that a plasmon with greater ejection speed has a shorter lifetime, which can be observed in simulations.

The final length of a plasmon is not related to its shape and depends on the initial conditions of the plasmon.

We acknowledge support from PAPIIT-UNAM grants IN-109518 and IG-100218. P.R.R.-O. acknowledges scholarship from CONACyT-México and financial support from COZCyT. We thank the anonymous referee for helpful comments and corrections.

Appendix Speed of Sound

Consider a supersonic flow with velocity v_2 and density ρ_2 interacting with a medium at rest with density ρ_1 . The interaction produces two shocks S_1 and S_2 (see Figure 8). Between the shocks there is a growing region that has a uniform velocity v_c and uniform pressure P . S_1 , the forward shock, moves with velocity v_{s1} and runs into the medium at rest, accelerating it to the velocity v_c , while S_2 , the reverse shock, moves with velocity v_{s2} into the impinging flow decelerating it to the same velocity v_c . The region has two

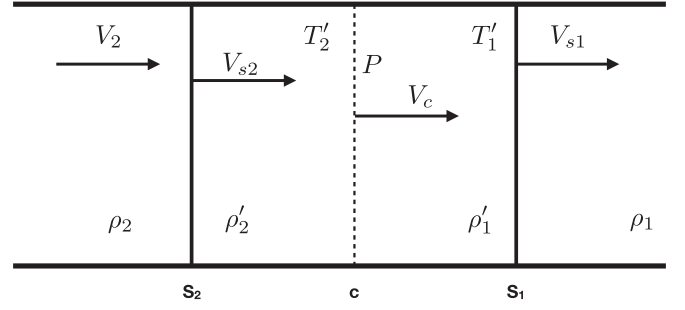


Figure 8. Scheme of the flow configuration produced by the interaction of a highly supersonic flow 2 with a gas at rest 1.

parts: one has density ρ'_2 and temperature T'_2 and is filled by shocked flow 2, while the other part is filled by shocked medium 1 and has density ρ'_1 and temperature T'_1 . Note that the pressure of both regions is, however, the same. These two regions are separated by a contact discontinuity C . We further assume that the shocks are strong and parallel. On a frame of reference moving with shock S_2 , we can write,

$$\rho'_2 = \frac{\gamma + 1}{\gamma - 1} \rho_2, \quad (29)$$

$$v'_2 = \frac{\gamma - 1}{\gamma + 1} (v_2 - v_{s2}) = v_c - v_{s2}, \quad (30)$$

and

$$P = \frac{2}{\gamma + 1} \rho_2 (v_2 - v_{s2})^2, \quad (31)$$

where v'_2 is the post- S_2 shock flow velocity in this frame of reference and γ is the ratio of specific heats.

Now, in a frame of reference that moves with shock S_1 , the jump conditions across the shock gives,

$$\rho'_1 = \frac{\gamma + 1}{\gamma - 1} \rho_1, \quad (32)$$

$$v'_1 = \frac{\gamma - 1}{\gamma + 1} (-v_{s1}) = v_c - v_{s1}, \quad (33)$$

and

$$P = \frac{2}{\gamma + 1} \rho_1 (-v_{s1})^2, \quad (34)$$

where v'_1 is the post- S_1 shock velocity in this frame of reference.

From (31) and (34) we find

$$v_2 - v_{s2} = \beta v_{s1}, \quad (35)$$

where $\beta = (\rho_1/\rho_2)^{\frac{1}{2}}$.

Combining (35) with (30), (33), and (34) we find

$$v_c = \frac{v_2}{1 + \beta} \quad (36)$$

$$v_{s1} = \frac{\gamma + 1}{2(1 + \beta)} v_2 \quad (37)$$

$$v_{s2} = \frac{2 + \beta(1 - \gamma)}{2(1 + \beta)} v_2 \quad (38)$$

$$P = \frac{\gamma + 1}{2(1 + \beta)^2} \rho_1 v_2^2 \quad (39)$$

Finally, the isothermal sound speed behind shock S_2 is,

$$c_2 = \sqrt{\frac{P}{\rho_2}} \quad (40)$$

$$c_2 = \left(\frac{\gamma - 1}{2}\right)^{1/2} \left(\frac{\beta}{1 + \beta}\right) v_2, \quad (41)$$

where we have used (29) and the definition of β .

We can use Equation (40) to estimate the sound speed of the gas that was left behind by the reverse shock (shock S_2); that is the sound speed inside the plasmon. For this, we identify the impinging flow in the model presented in this with the original clump. So, if v_0 and ρ_{cl} are the launch velocity and density of the clump, respectively, then, we take, $v_2 = v_0$, $\rho_2 = \rho_{cl}$, and ρ_1 equal to the density of the ambient medium through which the plasmon is moving ρ_a . Then, c_2 will be the sound speed inside the plasmon c , while v_c (from Equation (36)) will be the initial velocity of the plasmon v_0 . Substituting in Equation (41) we find,

$$c = v_0 \left(\frac{\gamma - 1}{2}\right)^{1/2} \beta. \quad (42)$$

ORCID iDs

A. Rodríguez-González  <https://orcid.org/0000-0002-2606-8527>

References

- Bally, J. 2016, *ARA&A*, 491, 54
 Bally, J., Cunningham, N. J., Moeckel, N., et al. 2011, *ApJ*, 113, 727
 Cantó, J., Espresate, J., Raga, A. C., & D'Alessio, P. 1998, *MNRAS*, 1041, 296
 Cantó, J., & Raga, A. 1991, *ApJ*, 372, 646
 Castellanos-Ramírez, A., Rodríguez-González, A., Rivera-Ortiz, P. R., et al. 2018, *RMxAA*, 54, 409
 Daly, R. A. 1994, *ApJ*, 38, 426
 Daly, R. A. 1995, *ApJ*, 580, 454
 De Young, D. S., & Axford, W. I. 1967, *Natur*, 129, 216
 Esquivel, A., Raga, A. C., Cantó, J., et al. 2010, *ApJ*, 725, 1466
 Henney, W. J., Arthur, S. J., de Colle, F., & Mellema, G. 2009, *MNRAS*, 157, 398
 Kahn, F. D. 1980, *A&A*, 83, 303
 Kosiński, R., & Hanasz, M. 2007, *MNRAS*, 861, 376
 Raga, A., Cabrit, S., & Cantó, J. 1995, *MNRAS*, 273, 422
 Raga, A. C., Cantó, J., Curiel, S., & Taylor, S. 1998, *MNRAS*, 738, 295
 Raga, A. C., & Reipurth, B. 2004, *RMxAA*, 15, 40
 Taylor, D., Dyson, J. E., & Axon, D. J. 1992, *MNRAS*, 351, 255
 Toro, E. F., Spruce, M., & Speares, W. 1994, *ShWav*, 4, 25
 Ubachukwu, A. A., Okoye, S. E., & Onuora, L. I. 1991, *ApJ*, 56, 383
 Veilleux, S., Tully, R. B., & Bland-Hawthorn, J. 1993, *AJ*, 1318, 105
 Yalinewich, A., & Sari, R. 2016, *ApJ*, 177, 826
 Zapata, L. A., Schmid-Burgk, J., Ho, P. T. P., Rodríguez, L. F., & Menten, K. M. 2009, *ApJL*, L45, 704